Fusion studies in ^{35,37}Cl + ^{181}Ta reactions via evaporation residue cross section measurements

P. V. Laveen [1,*] E. Prasad,[1,†] N. Madhavan,[2] A. K. Nasirov [3] J. Gehlot [2] S. Nath [2] G. Mandaglio [4,5] G. Giardina,[4]
A. M. Vinodkumar [6] M. Shareef,[1] A. Shamlath,[1] S. K. Duggi,[7] P. Sandya Devi,[7] Tathagata Banerjee,[2,‡] M. M. Hosamani,[8]
Khushboo,[9] P. Jisha [3] Neeraj Kumar,[9] Priya Sharma [10] and T. Varughese[2]

[1]*Department of Physics, School of Physical Sciences, Central University of Kerala, Kasaragod 671316, India*
[2]*Inter University Accelerator Centre, Aruna Asaf Ali Marg, New Delhi 110067, India*
[3]*BLTP, Joint Institute for Nuclear Research, Joliot-Curie 6, Dubna 141980, Russia*
[4]*Dipartimento MIFT - Universitá degli Studi di Messina, Viale F.S. D'Alcontres 31, Messina 98166, Italy*
[5]*INFN Sezione di Catania, Via Santa Sofia 64, Catania 95123, Italy*
[6]*Department of Physics, University of Calicut, Calicut 673635, India*
[7]*Department of Nuclear Physics, Andhra University, Visakhapatnam 530003, India*
[8]*Department of Physics, Karnatak University, Dharwad 580003, India*
[9]*Department of Physics and Astrophysics, University of Delhi, Delhi 110007, India*
[10]*Department of Physics, Panjab University, Chandigarh 160014, India*

The fusion evaporation residue (ER) excitation function has been measured for ^{35,37}Cl + ^{181}Ta reactions at energies above the Coulomb barrier. The measurements were performed using the HYbrid Recoil mass Analyzer at IUAC, New Delhi. Comparable ER cross sections have been observed in both reactions and there is no isotopic dependence. Measured ER cross sections were compared with theoretical calculations employing the dinuclear system model at projectile and target nuclei interaction and statistical model for the deexcitation of the formed compound nucleus. Larger ER cross sections at the complete deexcitation cascade of the formed compound nucleus are noticed in both reactions at higher excitation energies ($E^* > 80$ MeV) over the calculated results. Fusion probability varies from 95% to 40% in the excitation energy range of the study. No appreciable difference in the fusion probability is noticed in the two reactions. Comparison of our results with other reactions populating ^{216}Th shows a very strong entrance channel dependence.

I. INTRODUCTION

The identification of the residual nucleus known as evaporation residue (ER) is the definite confirmation of the production of heavy and superheavy nuclei in superheavy element research [1–3]. While the formation cross sections of the ERs are of the order of hundreds of millibarns in medium heavy nuclei, they drop to picobarns or femtobarns in the superheavy region. Though fission is the dominant decay mode in heavy nuclei, very low ER production cross section in heavy and superheavy nuclei is not solely due to this fission competition.

The formation of ERs is often regarded as a three-step process for simplicity: the capture, fusion, and survival of the fused system against fission [4]. Hence, the ER formation cross section (σ_{ER}) can be written as $\sigma_{ER} = \sigma_{cap} \times P_{CN} \times W_{sur}$, where σ_{cap}, P_{CN}, and W_{sur} represent the capture cross section, probability of the compound nucleus (CN) formation, and the survival probability of CN against fission,

respectively. While capture and fusion cross sections are of similar magnitude in lighter systems ($P_{CN} = 1$), significant hindrance in fusion is observed in heavy systems ($P_{CN} < 1$). This hindrance is attributed to the presence of noncompound nuclear (NCN) processes such as quasifission [5–9], fast fission [10–12], and preequilibrium fission [13]. The survival probability against fission also varies from $W_{sur} = 1$ to $W_{sur} < 1$, with increasing mass, excitation energy, angular momentum, etc.

Onset of NCN processes reduces the fusion probability. Reduction in ER cross section [6,14,15] is also noticed in more symmetric reactions compared to the asymmetric projectile-target combinations forming the same CN. Among the different NCN processes, quasifission is a dominant process at energies near the Coulomb barrier and competes strongly with fusion. The competition between the NCN processes and fusion defines P_{CN}. Though there are different prescriptions available for estimating the P_{CN} [16–20], the results of such calculations vary significantly from experimental results. Significant variations in P_{CN} have also been observed with increasing mass and excitation energy of the nuclei of interest. A systematic study using available ER cross section data in the 170–220 a.m.u. [20] mass region outlined approximate boundaries from where P_{CN} deviates from unity.

*laveenpv@cukerala.ac.in
†Corresponding author: prasadenair@cukerala.ac.in
‡Present address: Flerov Laboratory of Nuclear Reactions, Joint Institute for Nuclear Research, Dubna 141980, Russia.

While NCN processes play a vital role in deciding the P_{CN}, the survival probability W_{sur} against fission depends on factors like N/Z, fissility, shell effects, etc. Generally larger ER cross sections are observed with increase in N/Z values along an isotopic chain [15,21]. This is due to the lower fissility in systems with larger N/Z and also due to the lower binding energy of the neutrons in heavier isotopes; both favor particle evaporation and subsequent formation of ER. A difference from this general trend is, however, noticed in some cases [22].

Shell effects are also known to enhance the survival against fission. However, such effects are expected to vanish at high excitation energies. The stability of superheavy elements against fission is believed to be due to the microscopic shell stabilizations [1,23]. Though shell closure is expected to increase the fission barrier heights, collective enhancements in level density (CELD) and deformation effects are also supposed to influence fission and hence W_{sur}.

Though there is experimental evidence on stabilizing effects of $Z = 82$ [24], the stabilizing effect of $N = 126$ in fusion is not very clear [25–28]. ER studies in $^{19}F + ^{194,196,198}Pt$ reactions reported [29] a very low survival against fission in ^{213}Fr where the CN has $N = 126$, for example. It is reported [30] that shell stabilization in the actinide region is less significant due to the collective enhancements in level density.

Fusion dynamics in reactions forming various isotopes of thorium were explored extensively in recent years [22,31–33]. Fusion studies in $^{86}Kr + ^{130,136}Xe$ showed larger (almost 500 times) ER cross section in the reaction forming ^{222}Th compared to ^{216}Th, even though the latter is formed with $N = 126$. This was attributed mainly to the neutron excess in ^{222}Th compared to ^{216}Th [31]. Studies in the $^{40}Ar + ^{176}Hf$, $^{86}Kr + ^{130}Xe$, and $^{124}Sn + ^{92}Zr$ reactions explored the role of entrance channels, and angular momenta in fusion leading to CN ^{216}Th. Onset of quasifission is noticed in these reactions. A recent ER study in reactions forming ^{214}Th [22] reported larger ER cross sections in $^{18}O + ^{206}Pb$ compared with $^{16}O + ^{208}Pb$ at higher excitations.

We studied the fusion in $^{216,218}Th$ nuclei in this work, by measuring the total ER cross sections. The produced CN differ by two neutrons in this case, and one of the CN (^{216}Th) is populated with a major neutron shell closure at $N = 126$. Apart from these, ^{216}Th is populated with a $Z_P Z_T$ lower than the reactions studied in Ref. [31]. Also the CN is falling in the boundary region where P_{CN} is found to deviate from unity [20]. Hence, present reactions become good candidates to elucidate the dynamics of fusion and quasifission further in thorium isotopes.

The paper is structured as follows. The experimental details are presented in Sec. II, followed by the data analysis and experimental results in Sec. III. Theoretical calculations performed in the present study are discussed in Sec. IV. Interesting findings of this work are presented in Sec. V.

II. EXPERIMENTAL DETAILS

The measurements were performed at the Inter University Accelerator Centre (IUAC), New Delhi. Pulsed $^{35,37}Cl$ beams with a pulse separation of 2 μs from the 15 UD Pelletron
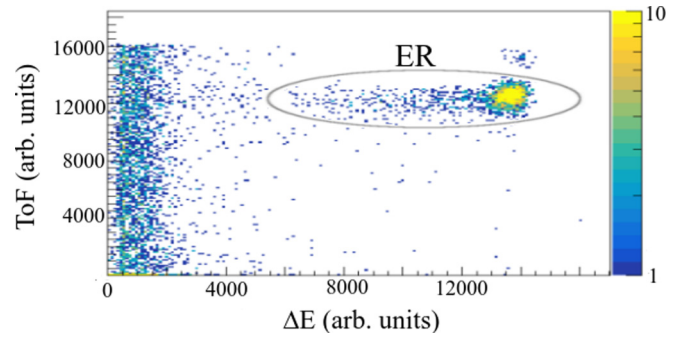

FIG. 1. The ΔE versus ToF spectrum at 225.7 MeV beam energy at the center of the target for the $^{35}Cl + ^{181}Ta$ reaction. ERs are shown inside the elliptical gate.

accelerator were further boosted in energy using the superconducting linear accelerator (sc-LINAC) before bombarding with the ^{181}Ta target mounted in the target chamber of HYbrid Recoil mass Analyzer (HYRA) [34]. The targets used have an average thickness of 170 μg/cm^2 evaporated on 20 μg/cm^2 thick carbon backing [35], fabricated in the target laboratory of IUAC. The measurements were performed in the beam energy range of 169.7–236.6 MeV, at the center of the target.

The ERs formed in the fusion reactions were separated from the intense beam background using HYRA. This separator is capable of operating in vacuum mode as well as in gas-filled mode. The gas-filled mode of HYRA was used in the present measurements, which offers better transmission efficiency over the vacuum-mode due to the inherent velocity and charge state focusing in the gas-filled magnetic separator. Helium gas at an optimized gas pressure of 0.15 Torr was used in HYRA as fill gas. A carbon foil of 650 μg/cm^2 thickness was used to separate the beam line vacuum from the gas-filled region of HYRA.

The magnetic configuration of HYRA (first phase used in the present study) is Q1Q2-MD1-Q3-MD2-Q4Q5, where Q stands for the magnetic quadrupole and MD for the magnetic dipole. The magnetic field values of these magnets were first calculated using a simulation [36] and were then set after scanning the field values around calculated values for the maximum transmission. Details of this procedure are reported elsewhere [15,37,38]. The optimized field values were within 5–10% of the calculated values at all energies.

The ERs reaching the focal plane of HYRA were detected using a position sensitive multiwire proportional counter (MWPC) of active area 6 inch × 2 inch. This detector was operated with isobutane at a pressure of 2.5 mbar and was isolated from the gas-filled region of HYRA using a mylar foil of 0.5 μm thickness. The gas detector provided position (both X and Y), time of arrival, and energy loss (ΔE) signals.

In order to improve the particle identification at the focal plane detector, a time-of-flight (ToF) spectrum was generated using the MWPC timing signal as the start and an RF pulse as the stop. The two-dimensional spectrum generated from the ΔE and ToF for the $^{35}Cl + ^{181}Ta$ is shown in Fig. 1 where the ERs are seen (shown inside the elliptical gate) unambiguously separated from other possible particles reaching the focal plane.
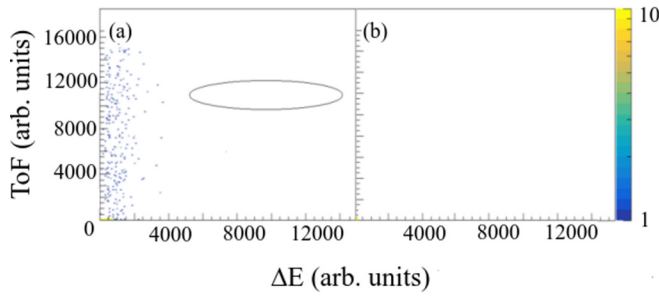
FIG. 2. Panel (a) shows the ΔE versus ToF spectrum at 225.7 MeV beam energy for the ^{35}Cl beam with blank target. Panel (b) shows the two-dimensional spectra for background runs.

The target chamber facilitates two silicon surface barrier detectors (SBDs) to record the elastically scattered beams for the normalization of ER cross sections. These SBDs were placed at $\pm 25°$ with respect to the beam direction, which also enabled us to focus the beam at the center of the target. The data were collected and analyzed using CANDLE software [39].

To further ensure the absence of beamlike particles reaching the focal plane detector, separate runs were taken with a blank frame in the target position, with the same magnetic field settings for the ERs. The observed spectrum in the focal plane is shown in Fig. 2(a). In order to rule out any possible decay channels overlapping with the ERs, background runs were also taken with no beam hitting the target, soon after a few measurements. As the ERs are stopped after the MWPC detector, decaying particles in the direction of the MWPC will be registered in it. The focal plane spectrum obtained in such a run is shown in Fig. 2(b). These procedures confirmed the excellent beam rejection capability of HYRA and the absence of beamlike or decay events populated in the region where ERs were identified in Fig. 1.

III. TOTAL ER CROSS SECTIONS

The total ER cross section is obtained from the ER and elastic yields using the relation

$$\sigma_{ER} = \frac{Y_{ER}}{Y_M} \left(\frac{d\sigma}{d\Omega} \right)_R \Omega_M \frac{1}{\eta_{HYRA}}, \qquad (1)$$

where σ_{ER} represents the total ER cross section in mb, Y_{ER} is the number of ERs registered at the focal plane detector, Y_M is the number of elastically scattered beam particles registered in the monitor detector, $(\frac{d\sigma}{d\Omega})_R$ is the differential Rutherford scattering cross section in the laboratory system, Ω_M is the solid angle subtended by the monitor detector, η_{HYRA} is the transmission efficiency of HYRA.

The number of ERs reaching the focal plane depends crucially on the transmission efficiency of the separator. It depends on several parameters discussed in Ref. [37,40–42]. We followed the same method discussed in Ref. [37] for the calculation of η_{HYRA} in the present study, where ^{30}Si + ^{180}Hf [15] was used as the calibration reaction. The ER cross section for this calibration reaction was previously measured [15]. The overall uncertainty in the estimated total ER cross sections is $\leqslant 18\%$ in which η_{HYRA} contributes the maximum. The
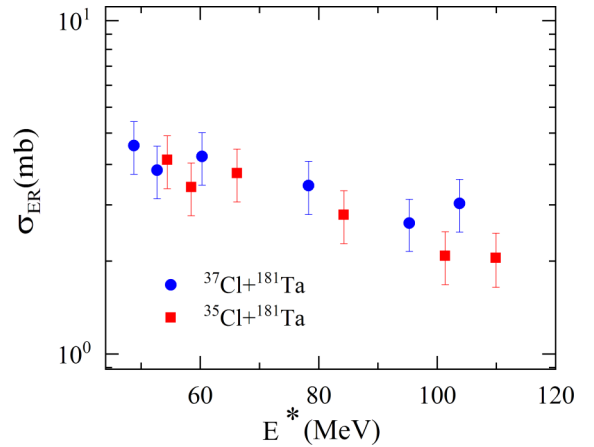

FIG. 3. Comparison of the measured ER cross sections for the ^{35}Cl + ^{181}Ta and ^{37}Cl + ^{181}Ta reactions as a function of the excitation energies.

measured ER cross sections for the ^{35,37}Cl + ^{181}Ta reactions at different excitation energies are shown in Fig. 3.

IV. THEORETICAL CALCULATIONS

In reactions forming medium heavy or heavy nuclei, capture inside the potential pocket need not guarantee complete fusion always. The system after capture may undergo reseparation into a quasifission channel in competition with the possibility of forming a mononuclear stage from which the system can reach the configuration of the excited compound nucleus. Hence, it is very important to follow the dynamics of the system right from the capture stage. The same treatment is followed in this work too, where the dinuclear system (DNS) model [43,44] is used for the capture calculations. The decay of the CN is simulated in the second stage of the calculations using the statistical treatment [31,45,46].

A. Cross sections of capture, fusion, and NCN processes

The calculation of the partial fusion cross section is described in many previous references [45,47]. The reaction dynamics at energies around the Coulomb barrier depends mainly on the capture probability of projectile-target system in the entrance channel. The capture stage is visualized by the full momentum transfer into the shape deformation and intrinsic degrees of freedom [32].

The capture cross section (σ_{cap}) is expressed as the sum of fusion cross section (σ_{fus}) and quasifission [5] cross section (σ_{qf}) in most of the cases. However, when the incident energy is very high, the angular momentum will be very large such that the fission barrier vanishes. In such cases, even if the system survives the quasifission competition, the formed mononucleus undergoes fission, referred to as fast fission [48]. While capture takes place for angular momentum $\ell = 0$ to $\ell = \ell_d$, fast fission dominates for angular momentum values between ℓ_B and ℓ_d, where ℓ_B is the angular momentum at which the fission barrier (B_{fis}) vanishes and ℓ_d is the maximum angular momentum that leads to capture. For instance, the calculated fission barrier for the CN ^{216}Th and ^{218}Th formed in
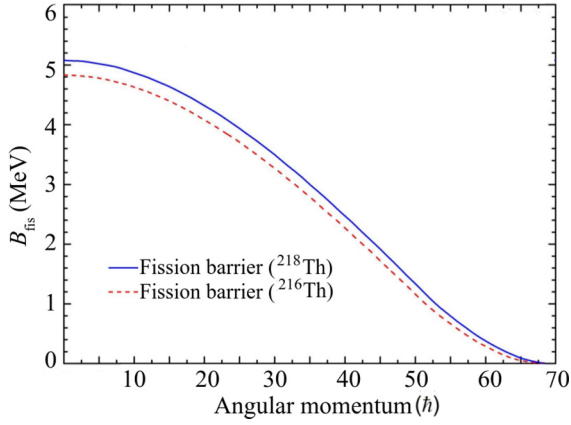
FIG. 4. The fission barrier for the compound nuclei ^{216}Th and ^{218}Th which are formed in the ^{35}Cl $+$ ^{181}Ta and ^{37}Cl $+$ ^{181}Ta reactions, respectively.

the ^{35}Cl $+$ ^{181}Ta and ^{37}Cl $+$ ^{181}Ta reactions, respectively, are shown in Fig. 4 as a function of angular momentum. It may be noticed that the fission barrier B_{fis} vanishes for the angular momentum values $\ell > \ell_B = 67\hbar$ in both cases. However, the calculations of partial cross section for the capture events have been performed up to $\ell = 120\hbar$ in this work. Hence, fast fission events are expected for ℓ above $67\hbar$.

The capture cross section is thus given by

$$\sigma_{\text{cap}}(E, \ell) = \sigma_{\text{fus}}(E, \ell) + \sigma_{\text{qf}}(E, \ell), \tag{2}$$

where

$$\sigma_{\text{fus}}(E, \ell) = \sigma_{\text{CN}}(E, \ell) + \sigma_{\text{fast}}(E, \ell) \tag{3}$$

and E is the center-of-mass energy. As the beam energy, deformation, and relative orientation of the colliding nuclei influence the capture, quasifission, and complete fusion cross sections, they are obtained by averaging the contributions calculated for the different orientation angles (α_1 and α_2) of the symmetry axis of the reacting nuclei [43,49]:

$$\sigma_i(E, \ell) = \int_0^{\pi/2} \sin\alpha_1 \int_0^{\pi/2} \sin\alpha_1 d\alpha_1 d\alpha_2 \sigma_i(E, \ell; \alpha_1, \alpha_2),$$

where i stands for capture, quasifission, and complete fusion. Orientation angles α_1 and α_2 are taken relative to the beam direction.

Capture cross section is given by

$$\sigma_{\text{cap}}(E, \alpha_1, \alpha_2) = \frac{\lambda^2}{4\pi} \sum_{\ell=0}^{\ell_d(E)} (2\ell+1)\mathcal{P}_{\text{cap}}(E, \ell; \{\alpha_i\}), \tag{4}$$

where λ and $\mathcal{P}_{\text{cap}}(E, \ell)$ denote the de Broglie wavelength and capture probability [47]. We assume a sharp cutoff approximation for the capture probability, where $\mathcal{P}_{\text{cap}}^{\ell}(E)$ is assumed to be equal to unity for the angular window $\ell_{min} \leqslant \ell \leqslant \ell_d$ and zero otherwise. Here, the maximum value of partial waves ℓ_d (leading to capture) is calculated by the solution of the equation of the relative motion of nuclei [31,43,47], and ℓ_{min} is the minimum value of ℓ leading to capture. For various reactions ℓ_{min} can even start from $\ell = 0$.

The complete fusion cross section σ_{fus} of the deformed mononucleus is obtained as

$$\sigma_{\text{fus}}(E; \alpha_1, \alpha_2) = \sum_{\ell=0}^{\ell_d(E)} \sigma_{\text{cap}}^{\ell}(E, \ell; \alpha_1, \alpha_2)$$
$$\times P_{CF}^{\ell}(E, \ell; \alpha_1, \alpha_2), \tag{5}$$

where $P_{CF}^{\ell}(E, \ell; \alpha_1, \alpha_2)$ is the complete fusion probability, while the quasifission cross section is obtained as the complementary part of σ_{fus},

$$\sigma_{\text{qf}}(E; \alpha_1, \alpha_2) = \sum_{\ell=0}^{\ell_d(E)} \sigma_{\text{cap}}^{\ell}(E, \ell; \alpha_1, \alpha_2)$$
$$\times \left[1 - P_{CF}^{\ell}(E, \ell; \alpha_1, \alpha_2) \right]. \tag{6}$$

The competition between complete fusion and quasifission processes during the DNS evolution is determined by the complete fusion probability P_{CF}^{ℓ} which is calculated by the expression [43,47]

$$P_{\text{CF}}^{\ell}(E_{\text{DNS}}^*, \ell; \{\alpha_i\}) = \sum_{Z_{\text{sym}}}^{Z_{\text{max}}} P_{\text{CF}}^{(Z)}(E_{\text{DNS}}^*, \ell; \{\alpha_i\})$$
$$\times Y_Z(E_{\text{DNS}}^*, \ell), \tag{7}$$

where $Z_{\text{sym}} = (Z_1 + Z_2)/2$ and Z_{max} corresponds to the point where the driving potential reaches its maximum, i.e., the value at which the intrinsic fusion barrier $B_{\text{fus}}^* = 0$ (see details in the Appendix); $Y_Z(E_{\text{DNS}}^*, \ell)$ is the charge distribution function [50] operating on the $P_{\text{CF}}^{(Z)}$ factor. The mass and charge distributions among the DNS fragments are calculated by solving the transport master equation [51]. Therefore, the part of the complete fusion cross section σ_{CF} (of the deformed mononucleus) that is transformed into the CN cross section σ_{CN} (of the statistically equilibrated system CN) is obtained as

$$\sigma_{\text{CN}}(E; \alpha_1, \alpha_2) = \sum_{\ell=0}^{\ell_B} \sigma_{\text{cap}}^{\ell}(E, \ell; \alpha_1, \alpha_2)$$
$$\times P_{CF}^{\ell}(E, \ell; \alpha_1, \alpha_2), \tag{8}$$

while the part going in fast fission is related to the angular momentum interval from ℓ_B to ℓ_d,

$$\sigma_{\text{fast}}(E; \alpha_1, \alpha_2) = \sum_{\ell=\ell_B}^{\ell_d(E)} \sigma_{\text{cap}}^{\ell}(E, \ell; \alpha_1, \alpha_2)$$
$$\times P_{CF}^{\ell}(E, \ell; \alpha_1, \alpha_2); \tag{9}$$

therefore, the CN formation probability P_{CN} corresponds to the ratio $\sigma_{\text{CN}}/\sigma_{\text{cap}}$.

The contour plots of partial fusion, fast fission, and quasifission cross sections of the ^{35}Cl $+$ ^{181}Ta (left panels) and ^{37}Cl $+$ ^{181}Ta (right panel) reactions are shown in Fig. 5, as a function of excitation energy (E^*) and angular momentum of the CN.
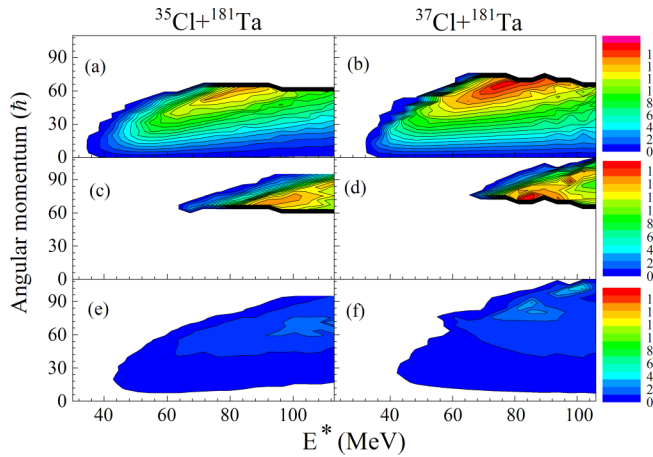
FIG. 5. Partial fusion [(a) and (b)], fast fission [(c) and (d)], and quasifission [(e) and (f)] cross sections (in units of mb/$\hbar$) for the ^{35}Cl + ^{181}Ta and ^{37}Cl + ^{181}Ta reactions, respectively, as a function of excitation energy and angular momentum.

B. Evolution in the potential energy surface (PES)

The PES, over which the system evolves, is computed from the binding energies of the constituents and the interaction potential energies between them [43]. The features of the PES mainly depend on the mass, charge, deformation, and microscopic structure of the interacting nuclei. These, in turn, influence the capture probability. The beam energy, angular momentum, and strength of dissipative forces are also found to influence capture probability and the subsequent formation of the DNS.

Another important factor that decides the reaction outcome is the sticking time of the DNS after capture. If the DNS does not stay together for a time sufficient enough for the equilibration of all degrees of freedom, nonequilibrated products such as quasifission will be formed, where the DNS splits into fissionlike fragments.

The PES is determined using the energy balance Q_{gg} between the CN and interacting nuclei; the nucleus-nucleus potential V is calculated for the ranges of angular momentum $\ell = 0$ to $\ell = \ell_d$ and orientation angles α_1 and α_2, as given in Refs [43,49], where the nuclear masses are obtained from Refs [52,53], for estimating Q_{gg}.

In Fig. 6, the PES calculated for the ^{35}Cl + ^{181}Ta reaction populating ^{216}Th is shown as an example, for $\ell = 0$. The capture, fusion, and one of the probable quasifission paths are shown in the figure. From such a PES calculated for a given ℓ, we calculate the driving potential U_{dr} by connecting all the minima in the PES, for all values of Z.

The calculated driving potential (U_{dr}) for the ^{35}Cl + ^{181}Ta (red dotted line) and ^{37}Cl + ^{181}Ta (blue solid line) reactions at $\ell = 60\hbar$ as a function of Z is shown in Fig. 7. The upward arrow (at $Z = 17$) indicates the entrance channel configuration of the projectile-target system. The intrinsic barrier (B^*_{fus}), which reduces the CN formation is shown in both cases relative to the entrance channel configuration. The height of this barrier depends on the charge and mass asymmetry and microscopic structure of the DNS fragments. As the features of the PES are greatly influenced by the deformation (both
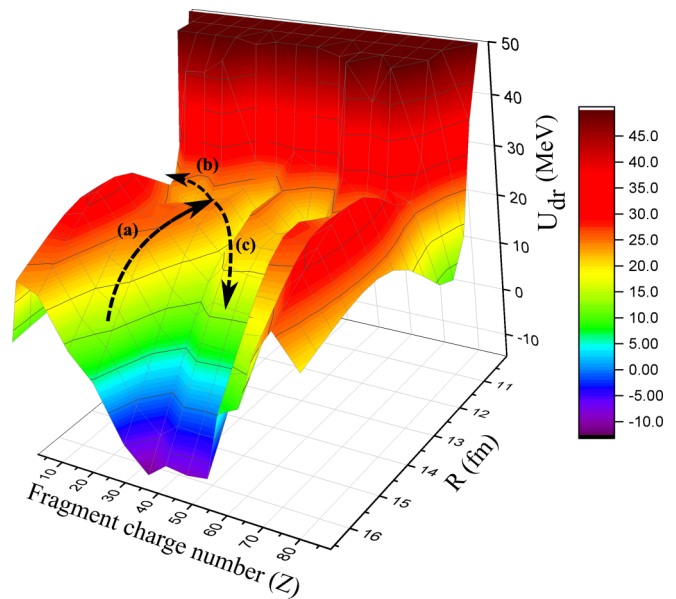

FIG. 6. PES (in MeV) calculated for the ^{35}Cl + ^{181}Ta reaction populating ^{216}Th is shown as a function of the distance (R) between the interacting nuclei and charge numbers (Z) of the fragments. The arrow (a) shows the capture path, (b) the fusion path, and (c) is one of the QF paths.

static and dynamic) and relative orientation of the colliding partners, the same is expected to be reflected in the height of B^*_{fus} in these reactions. It is observed that the B^*_{fus} is larger for the ^{35}Cl + ^{181}Ta reaction compared to that of ^{37}Cl + ^{181}Ta, implying a larger hindrance to fusion in the former case.

C. Decay of the CN: Statistical model analysis

The heavy CN populated in the reactions studied decay via fission and particle evaporation (charged particles and neutrons), producing fission fragments and evaporation residues,
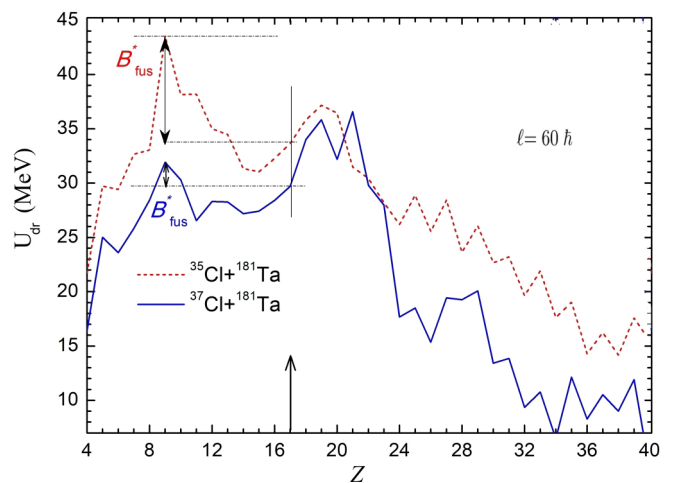

FIG. 7. The driving potentials calculated for dinuclear systems formed in the ^{35}Cl + ^{181}Ta and ^{37}Cl + ^{181}Ta reactions for orbital angular momentum $\ell = 60\hbar$ as a function of the fragment Z.

respectively. The decay of these CN is performed using statistical model analysis [54] for given E^* and angular momentum ℓ. The ER cross section at a given excitation energy E_x^* is obtained by summing the partial waves,

$$\sigma_{\text{ER}}^x(E_x^*) = \sum_{\ell=0}^{\ell_B} \sigma_{\text{ER}}^x(E_x^*, \ell), \tag{10}$$

where $\sigma_{\text{ER}}^x(E_x^*, \ell)$ denotes the partial cross section for the formation of ER after emitting charged and neutral particles and γ quanta from the intermediate stage during the evolution of CN with excitation energy E_x^* during each step x of the deexcitation process [45,54]. The evaporation begins from the CN stage, with $x = 0$. Here, the summation is carried out only up to $\ell = \ell_B$, as fast fission dominates beyond ℓ_B. Also,

$$\sigma_{\text{ER}}^x(E_x^*, \ell) = \sigma_{\text{ER}}^{x-1}(E_{x-1}^*, \ell) W_{\text{sur}}^x(E_x^*, \ell), \tag{11}$$

where $W_{\text{sur}}^x(E^*, \ell)$ is the survival probability against fission of the xth intermediate nucleus during the deexcitation of the CN. Here, we used a shell corrected (δW) macroscopic parametrization for the fission barrier [55], where damping of shell effects with increase in excitation energy (hence temperature, T) and angular momentum [54] were also taken into consideration. Though both ground state and saddle point configurations contribute to the total δW, we only considered the shell corrections at the ground state configuration (δW_{gs}) in these calculations, as the microscopic corrections at the saddle (δW_{sad}) are much smaller due to large deformations at the saddle configuration.

The fission barrier is thus

$$B_{\text{fis}}(\ell, T) = B_{\text{fis}}^m(\ell) - \alpha(T) \times \beta(\ell) \times \delta W, \tag{12}$$

where

$$\alpha(T) = \left[1 + \exp\frac{(T - T_{\frac{1}{2}})}{d} \right]^{-1} \tag{13}$$

and

$$\beta(\ell) = \left[1 + \exp\left(\frac{\ell - \ell_{\frac{1}{2}}}{\Delta\ell} \right) \right]^{-1}. \tag{14}$$

Here, d and $\Delta\ell$ are the rate of vanishing of shell effects with increase in temperature and angular momentum, respectively. $T_{\frac{1}{2}}$ is the temperature at which the damping factor $\alpha(T)$ is reduced by half, and $\ell_{\frac{1}{2}}$ is value of ℓ at which $\beta(\ell)$ is reduced by half. In this work, we used $d = 0.3$ MeV, $T_{\frac{1}{2}} = 1.16$ MeV, $\Delta l = 3\hbar$ and $\ell_{\frac{1}{2}} = 20\hbar$ [32].

In this work, we define the excitation energy of the CN as $E^* = E + Q - E_{\text{rot}}$, where E is the energy available in the center-of-mass frame, Q is the ground state Q value, and E_{rot} is the rotational energy $E_{\text{rot}} = \ell(\ell + 1)\hbar^2/(2\mathcal{J})$, where $\mathcal{J}$ is the effective moment of inertia. The nuclear temperature is given by $T = \sqrt{\frac{E^*}{a}}$, where a is the intrinsic level density parameter.

V. RESULTS AND DISCUSSION

In this section, we compare the experimental ER cross sections with the theoretical results. Measured ER excitation functions presented in Fig. 3 show that the ER cross sections

TABLE I. The entrance channel, CN, charge asymmetry ($\eta = \frac{Z_T - Z_P}{Z_T + Z_P}$), mass asymmetry ($\alpha = \frac{A_T - A_P}{A_T + A_P}$), Businaro-Gallone mass asymmetry (α_{BG}), and effective fissility (χ_{eff}) for the reactions in the present work.

Reaction	CN	η	α	α_{BG}	χ_{eff}
^{35}Cl + ^{181}Ta	^{216}Th	0.62	0.676	0.876	0.621
^{37}Cl + ^{181}Ta	^{218}Th	0.62	0.660	0.875	0.609

are comparable within the experimental uncertainties for both the reactions studied. No obvious isotopic dependence is observed in the measured ER cross sections in the excitation energy chosen in this study. The details of entrance channel properties of the two reactions are tabulated in Table I.

In Fig. 8, we compare the measured total ER cross sections with the theoretical results. It may be noticed that the experimental results are in good agreement with the calculations up to $E^* = 84$ MeV, where $E^* = E + Q - E_{\text{rot}}$. Larger ER cross sections are noticed at higher excitation energies, with significant deviations from calculations with increasing E^*. Calculated capture, fusion, quasifission, fast fission, and $\sum xn$ channel cross sections are also presented in the same figure.

At lower excitation energies, the capture and fusion cross sections overlap considerably, suggesting less significance of NCN processes in the ^{35}Cl + ^{181}Ta reaction. Among the probable NCN processes, quasifission is significant at low E^*. Fast fission becomes significant only at $E^* > 50$ MeV and it takes over quasifission at $E^* > 80$ MeV. This delayed onset of fast fission is obvious as it results from higher angular momentum events, whereas quasifission happens at all angular momentum values. The onset of quasifission at lower E^* may also be due to the deformation of the target, as deformation alignment reduces the barrier and allows contact at near barrier energies.

The experimental ER cross sections, calculated ER cross sections, fusion, quasifission, fast fission, and $\sum xn$ channel cross sections for the ^{37}Cl + ^{181}Ta reaction are shown in Fig. 9. A similar feature may be observed in the ER cross
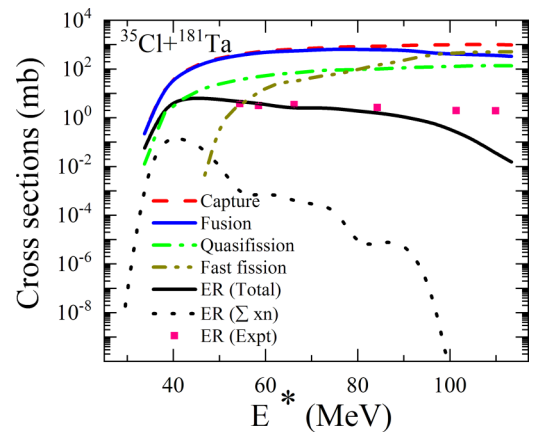

FIG. 8. Total ER cross sections are compared with the calculations (solid black line) for the ^{35}Cl + ^{181}Ta reaction. Calculated capture, fusion, quasifission, fast fission, and $\sum xn$ channel cross sections are also shown in the same figure, as a function of excitation energy.
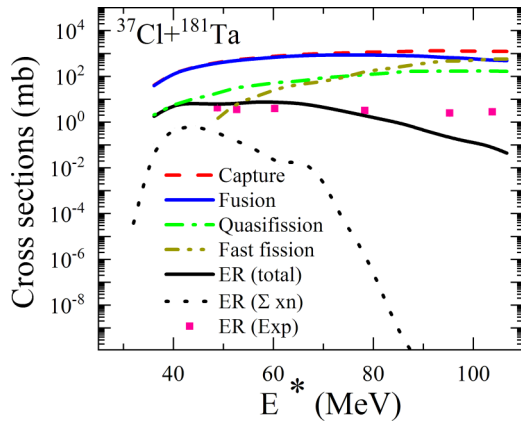
FIG. 9. Same as in Fig. 8, but for the ^{37}Cl + ^{181}Ta reaction.

FIG. 10. Capture, fusion, quasifission, and fast fission cross sections for the ^{35}Cl + ^{181}Ta and ^{37}Cl + ^{181}Ta reactions, as a function of excitation energy.

sections at high E^* here as well, with the experimental results deviating significantly from the calculated values.

Thus, a common feature in the ER cross sections of both ^{35,37}Cl + ^{181}Ta reactions is the enhanced total ER cross sections at higher E^* over the calculated results. Also, the total ER cross sections do not drop significantly with increase in excitation energy. Such a trend has previously been reported in the ^{28,30}Si + ^{180}Hf reactions [15] and in the ^{12}C + ^{197}Au reaction [56]. It is shown that a calculation assuming fusion following projectile breakup reasonably reproduces the experimental cross sections in Ref. [15]. It was mentioned that such processes stem from higher angular momentum collisions [56,57].

Surprisingly, large ER cross section (4.3 mb) is reported in the ^{40}Ar + ^{181}Ta reaction at an excitation energy of 371 MeV [58], where the ER cross sections were measured at GSI using the SHIP [59] facility. A comparison of the reduced ER cross sections of ^{16}O + ^{186}W and ^{48}Ca + ^{154}Sm reactions [60] revealed fusion hindrance and hence a lower ER cross section in the latter reaction compared to the former one at lower excitation energies. This hindrance was attributed to quasifission in the more symmetric ^{48}Ca + ^{154}Sm reaction, particularly at low excitations. However, it is seen that this hindrance to fusion disappears at E^* around 100 MeV, and both reactions yielded similar ER cross sections. It was argued that the quasifission process which is responsible for the reduced ER yield in the ^{48}Ca + ^{154}Sm reaction is no longer present at such high E^* and other possible NCN processes such as fast fission or precompound fission compete with fusion-fission without affecting the ER cross sections. The same paper [60] also called for more experimental studies at higher excitation energy in heavier systems to understand this observation unambiguously.

In Figs. 8 and 9, one may notice that the total ER cross section (black solid line) is much higher compared to the sum of xn channels (black dotted line) indicating the presence of proton and alpha evaporation channels dominating at higher excitation energies. Statistical model decay analysis also show the dominance of such channels at high E^*. Study of these channels may be significant in nucleosynthesis processes. As a channel-wise measurement is beyond the scope of present
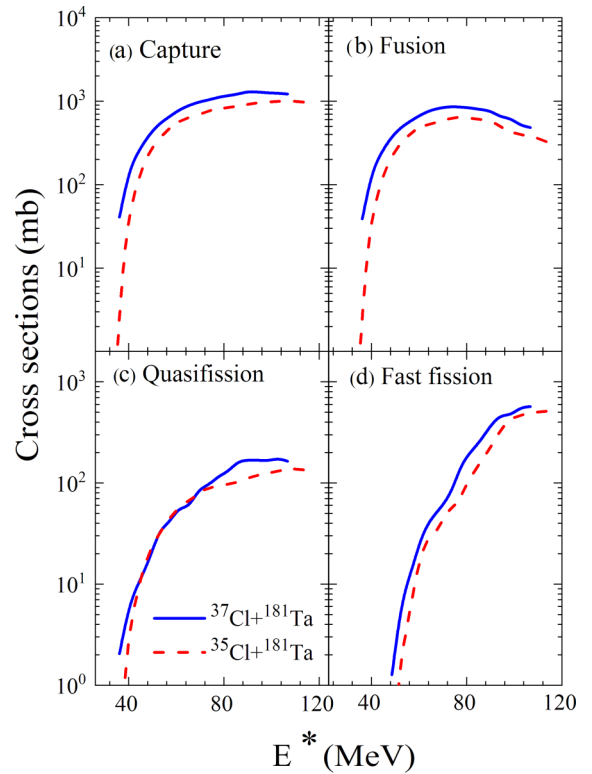
study, more experimental investigations in this excitation energy range is called for to explore this observation.

Next, we compare the calculated capture, fusion, quasifission, and fast fission cross sections of ^{35,37}Cl + ^{181}Ta reactions in Fig. 10. Larger capture, fusion, and fast fission probabilities are noticed for the ^{37}Cl + ^{181}Ta reaction compared to ^{35}Cl + ^{181}Ta at all energies. This may be due to the more negative Q value in the former reaction ($Q = -92.57$ MeV) compared to the latter (-87.75 MeV), so that the potential well can accommodate more partial waves in the former case.

The lower fusion cross section in the ^{35}Cl + ^{181}Ta reaction compared to ^{37}Cl + ^{181}Ta in Fig. 10(b) indicates a relative fusion hindrance in the ^{35}Cl + ^{181}Ta reaction. This is due to the larger B^*_{fus} in ^{35}Cl + ^{181}Ta as presented in Fig. 7. A significant quasifission cross section is noticed in both reactions, even though the charge product $Z_P Z_T$ (= 1241) is less than 1600 in both cases. Onset of quasifission in reactions with $Z_P Z_T < 1600$ are reported earlier in ER [6,14,15,61] and fission studies [62–65]. The quasifission cross sections appear to be the same in both reactions for $E^* < 80$ MeV. This may be due to the fact that the factors on which quasifission depends, such as $Z_P Z_T$, deformation of the target nucleus, fissility of the compound system, etc., remain the same in both cases. The difference in quasifission cross sections observed at higher excitation may be due to the difference in the angular momentum populated in the composite system after collision. Unlike quasifission, fast fission cross sections are larger in the ^{37}Cl + ^{181}Ta reaction throughout the energy range compared
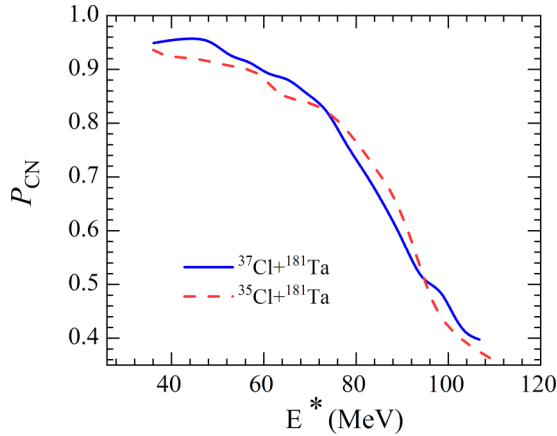
FIG. 11. P_{CN} for the ^{35,37}Cl + ^{181}Ta reactions as a function of excitation energy.

to ^{35}Cl + ^{181}Ta. This could be due to the larger angular momentum brought in by the heavier projectile.

The fusion probabilities (P_{CN}) for the two reactions are presented in Fig. 11 as a function of excitation energy. P_{CN} varies from 95% to 40% in the excitation energy range of 40–100 MeV. No marked difference in P_{CN} is noticed in the two reactions in this excitation energy range. The reduction in P_{CN} with increasing energy is due to the increase of B^*_{fus} with increase in angular momentum of the dinuclear system. Though increase in beam energy increases the number of partial waves that contribute to capture, the quasifission barrier (B_{qf}) decreases with increase in angular momentum since the depth of the potential well decreases with increasing ℓ.

Even though calculated fusion cross section is higher in ^{37}Cl + ^{181}Ta compared to ^{35}Cl + ^{181}Ta, measured total ER cross sections are comparable within the experimental uncertainties. This hints at a possibility that the fission survival probability is different in the two reactions: ^{216}Th ($N = 126$) formed through the ^{35}Cl + ^{181}Ta reaction has larger W_{sur} compared to ^{218}Th. Hence it is very important to measure the fission cross section of these nuclei in the E^* range of this study.

Finally, the capture and fusion cross sections obtained for the ^{35}Cl + ^{181}Ta ($Z_P Z_T = 1241$, $\alpha = 0.6759$) reaction is compared with ^{40}Ar + ^{176}Hf ($Z_P Z_T = 1296$, $\alpha = 0.6296$), ^{86}Kr + ^{130}Xe ($Z_P Z_T = 1944$, $\alpha = 0.2037$), and ^{124}Sn + ^{92}Zr ($Z_P Z_T = 2000$, $\alpha = 0.1481$) in Fig. 12, where all the reactions populate the same CN ^{216}Th. The x axis denotes the energy in the center-of-mass frame normalized by the Coulomb barrier. The data for ^{40}Ar + ^{176}Hf, ^{86}Kr + ^{130}Xe, and ^{124}Sn + ^{92}Zr were reproduced from Ref. [31]. A clear suppression in fusion is observed with increase in $Z_P Z_T$ (and decrease in mass asymmetry), indicating a strong entrance channel dependence in fusion. The fusion probability is significantly reduced in a more symmetric entrance channel due to NCN processes. The deviation observed from the general regularity expected between the ^{86}Kr + ^{130}Xe and ^{124}Sn + ^{92}Zr reactions is explained in terms of B^*_{fus} in Ref. [31]. It is noted that B^*_{fus} for the ^{86}Kr + ^{130}Xe reaction is higher than that of the ^{124}Sn + ^{92}Zr reaction, leading to a reduced fusion excitation function in the ^{86}Kr + ^{130}Xe reaction.
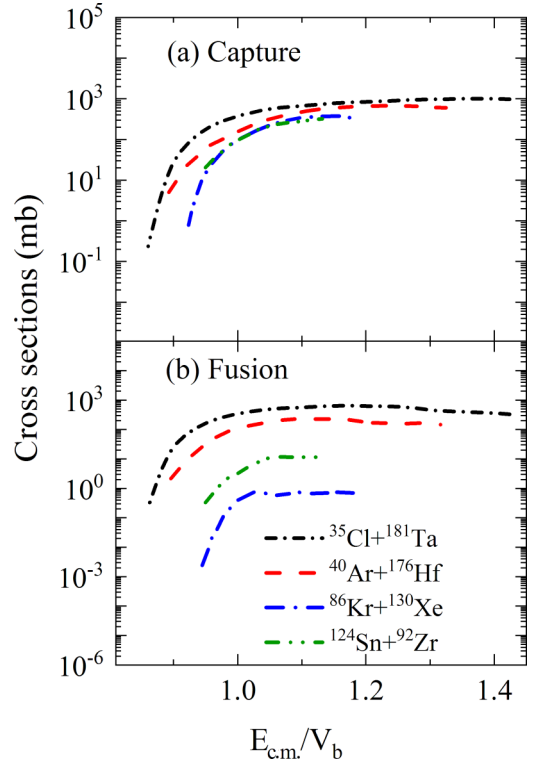

FIG. 12. The comparison of the calculated capture and fusion cross sections for the ^{35}Cl + ^{181}Ta reaction with ^{40}Ar + ^{176}Hf, ^{86}Kr + ^{130}Xe, and ^{124}Sn + ^{92}Zr reactions [31], as a function of the energy in the center-of-mass frame normalized by the respective Coulomb barrier.

VI. SUMMARY

ER cross sections for the ^{35,37}Cl + ^{181}Ta reactions were measured at IUAC using the HYRA facility. The measured ER cross sections do not show any isotopic dependence within the uncertainties.

The experimental results are compared with theoretical calculations incorporating the DNS and statistical model calculations. Both quasifission and fast fission processes contribute to the NCN processes in both reactions, even though $Z_P Z_T < 1600$. While quasifission is present at all energies, fast fission dominates at high excitations, and takes over quasifission at $E^* > 80$ MeV. The fusion probability varies from 95% to 40% in the E^* range of the present study. The decrease in P_{CN} with increasing energy is attributed to the decrease of quasifission barrier with increase in angular momentum.

Even though the calculated fusion cross section is larger for the ^{37}Cl + ^{181}Ta reaction, similar measured ER cross sections indicate that the survival probability W_{sur} is higher in the ^{35}Cl + ^{181}Ta reaction. The CN formed in the latter reaction has $N = 126$. In order to explore such a possibility of larger W_{sur} in ^{216}Th (which is more fissile than ^{218}Th), fission measurements are warranted in these reactions.

The comparison of the capture and fusion cross sections of four reactions forming the CN ^{216}Th clearly demonstrates the entrance channel effect in the fusion dynamics of reactions forming ^{216}Th. Hindrance to fusion increases with increase

in charge product (and decrease in mass asymmetry) in the entrance channel.

Measured ER cross sections are reasonably reproduced by the calculations up to 80 MeV of excitation energy in both cases. Significant difference between the experimental and calculated cross sections is noticed at excitation energies above 80 MeV. A similar trend in ER cross sections had been noticed in a few previous measurements. Though different explanations are suggested [15,60], this observation needs more experimental and theoretical investigations.

APPENDIX

In the present model, the fusion and quasifission cross sections were calculated by the expression [31,43,66]

$$\sigma_{\text{fus}}(E) = \sum_{\ell=0}^{\ell_d} \langle \sigma_{\text{fus}}(E, \ell) \rangle, \tag{A1}$$

where $\langle \sigma_{\text{fus}}(E, \ell) \rangle$ is calculated as

$$\sigma_{\text{fus}}(E, \ell; \{\alpha_i\}) = \sigma_{\text{cap}}(E, \ell; \{\alpha_i\}) P_{\text{CF}}^\ell(E, \ell; \{\alpha_i\}), \tag{A2}$$

where

$$P_{\text{CF}}^\ell(E_{\text{DNS}}^{*(Z)}, \ell; \{\alpha_i\}) = \sum_{Z_{\text{sym}}}^{Z_{\text{max}}} P_Z(E_{\text{DNS}}^{*(Z)}, \ell, \{\alpha_i\})$$

$$\times P_{\text{CF}}^{(Z)}(E_{\text{DNS}}^{*(Z)}, \ell; \{\alpha_i\}) \tag{A3}$$

and where $P_{\text{CF}}^{(Z)}(E_{\text{DNS}}^{*(Z)}, \ell; \{\alpha_i\})$ is the fusion probability of the dinuclear system fragments with the charge asymmetry Z; $E_{\text{DNS}}^{*(Z)}$ is the excitation energy of the DNS:

$$E_{\text{DNS}}^{*(Z)} = E + Q_Z - \Delta V_m(Z, R_m(Z)), \tag{A4}$$

which is determined by the collision energy E in the center of mass; the minimum of the potential well $\Delta V_m(Z, R_m(Z)) = V_m(Z, R_m(Z)) - V_m(Z_P, R_m(Z_P))$ is a change of the nucleus-nucleus interaction between fragments of the DNS with the charge asymmetry $Z_1 = Z(Z_2 = Z_{\text{CN}} - Z)$ relative to the entrance channel; and energy balance Q_Z appears at the nucleon transfer between nuclei: $Q_Z = \{M_1(Z) + M_2(Z_2) - [M_P(Z_P) + M_T(Z_T)]\}c^2$, where $M_1(Z)$ and $M_2(Z_2)$ are the mass (charge) numbers of fragments of dinuclear system, while M_P (Z_P) and M_T (Z_T) are the ones of the projectile (P) and target (T) nuclei [15,32].

[1] Y. Oganessian, J. Phys. G: Nucl. Part. Phys. **34**, R165 (2007).

[2] J. Hamilton, S. Hofmann, and Y. Oganessian, Annu. Rev. Nucl. Part. Sci. **63**, 383 (2013).

[3] S. Hofmann, J. Phys. G: Nucl. Part. Phys. **42**, 114001 (2015).

[4] V. I. Zagrebaev, Phys. Rev. C **64**, 034606 (2001).

[5] J. Toke, R. Bock, G. Dai, A. Gobbi, S. Gralla, K. Hildenbrand, J. Kuzminski, W. Müller, A. Olmi, H. Stelzer, B. Back, and S. Bjørnholm, Nucl. Phys. A **440**, 327 (1985).

[6] A. C. Berriman, D. J. Hinde, M. Dasgupta, C. R. Morton, R. D. Butt, and J. O. Newton, Nature (London) **413**, 144 (2001).

[7] B. B. Back, Phys. Rev. C **31**, 2104 (1985).

[8] B. B. Back, P. B. Fernandez, B. G. Glagola, D. Henderson, S. Kaufman, J. G. Keller, S. J. Sanders, F. Videbæk, T. F. Wang, and B. D. Wilkins, Phys. Rev. C **53**, 1734 (1996).

[9] W. Q. Shen, J. Albinski, A. Gobbi, S. Gralla, K. D. Hildenbrand, N. Herrmann, J. Kuzminski, W. F. J. Müller, H. Stelzer, J. Töke, B. B. Back, S. Björnholm, and S. P. Sørensen, Phys. Rev. C **36**, 115 (1987).

[10] C. Ngo, Prog. Part. Nucl. Phys. **16**, 139 (1986).

[11] C. Lebrun, F. Hanappe, J. LeColley, F. Lefebvres, C. Ngô, J. Péter, and B. Tamain, Nucl. Phys. A **321**, 207 (1979).

[12] C. Ngo, C. Gregoire, B. Remaud, and E. Tomasi, Nucl. Phys. A **400**, 259 (1983).

[13] V. S. Ramamurthy and S. S. Kapoor, Phys. Rev. Lett. **54**, 178 (1985).

[14] R. N. Sagaidak, G. N. Kniajeva, I. M. Itkis, M. G. Itkis, N. A. Kondratiev, E. M. Kozulin, I. V. Pokrovsky, A. I. Svirikhin, V. M. Voskressensky, A. V. Yeremin, L. Corradi, A. Gadea,

A. Latina, A. M. Stefanini, S. Szilner, M. Trotta, A. M. Vinodkumar, S. Beghini, G. Montagnoli, F. Scarlassara, D. Ackermann, F. Hanappe, N. Rowley, and L. Stuttgé, Phys. Rev. C **68**, 014603 (2003).

[15] A. Shamlath, E. Prasad, N. Madhavan, P. V. Laveen, J. Gehlot, A. K. Nasirov, G. Giardina, G. Mandaglio, S. Nath, T. Banerjee, A. M. Vinodkumar, M. Shareef, A. Jhingan, T. Varughese, D. Kumar, P. S. Devi, Khushboo, P. Jisha, N. Kumar, M. M. Hosamani, and S. Kailas, Phys. Rev. C **95**, 034610 (2017).

[16] R. Yanez, W. Loveland, J. S. Barrett, L. Yao, B. B. Back, S. Zhu, and T. L. Khoo, Phys. Rev. C **88**, 014606 (2013).

[17] R. S. Naik, W. Loveland, P. H. Sprunger, A. M. Vinodkumar, D. Peterson, C. L. Jiang, S. Zhu, X. Tang, E. F. Moore, and P. Chowdhury, Phys. Rev. C **76**, 054604 (2007).

[18] V. Zagrebaev and W. Greiner, Phys. Rev. C **78**, 034610 (2008).

[19] G. Giardina, A. K. Nasirov, G. Mandaglio, F. Curciarello, V. D. Leo, G. Fazio, M. Manganaro, M. Romaniuk, and C. Saccá, J. Phys.: Conf. Ser. **282**, 012006 (2011).

[20] T. Banerjee, S. Nath, and S. Pal, Phys. Rev. C **91**, 034619 (2015).

[21] P. Sharma, B. R. Behera, R. Mahajan, M. Thakur, G. Kaur, K. Kapoor, K. Rani, N. Madhavan, S. Nath, J. Gehlot, R. Dubey, I. Mazumdar, S. M. Patel, M. Dhibar, M. M. Hosamani, Khushboo, N. Kumar, A. Shamlath, G. Mohanto, and S. Pal, Phys. Rev. C **96**, 034613 (2017).

[22] M. M. Hosamani, N. M. Badiger, N. Madhavan, I. Mazumdar, S. Nath, J. Gehlot, A. K. Sinha, S. M. Patel, P. B. Chavan, T. Varughese, V. Srivastava, M. M. Shaikh, P. S. Devi, P. V.

Laveen, A. Shamlath, M. Shareef, S. K. Duggi, P. V. M. Rao, G. N. Jyothi, A. Tejaswi, P. N. Patil, A. Vinayak, K. K. Rajesh, A. Yadav, A. Parihari, R. Biswas, M. Dhibar, D. P. Kaur, M. Ratna Raju, and J. Joseph, Phys. Rev. C **101**, 014616 (2020).

[23] Y. Oganessian and V. Utyonkov, Nucl. Phys. A **944**, 62 (2015), Special Issue on Superheavy Elements.

[24] A. N. Andreyev, M. Huyse, P. Van Duppen, C. Qi, R. J. Liotta, S. Antalic, D. Ackermann, S. Franchoo, F. P. Heßberger, S. Hofmann, I. Kojouharov, B. Kindler, P. Kuusiniemi, S. R. Lesher, B. Lommel, R. Mann, K. Nishio, R. D. Page, B. Streicher, i. c. v. Šáro, B. Sulignano, D. Wiseman, and R. A. Wyss, Phys. Rev. Lett. **110**, 242502 (2013).

[25] D. A. Mayorov, T. A. Werke, M. C. Alfonso, M. E. Bennett, and C. M. Folden, Phys. Rev. C **90**, 024602 (2014).

[26] D. Vermeulen, H.-G. Clerc, C.-C. Sahm, K.-H. Schmidt, J. G. Keller, G. Münzenberg, and W. Reisdorf, Z. Phys. A: At. Nucl. **318**, 157 (1984).

[27] A. Chaudhuri, T. K. Ghosh, K. Banerjee, S. Bhattacharya, J. Sadhukhan, S. Kundu, C. Bhattacharya, J. K. Meena, G. Mukherjee, A. K. Saha, M. A. Asgar, A. Dey, S. Manna, R. Pandey, T. K. Rana, P. Roy, T. Roy, V. Srivastava, P. Bhattacharya, D. C. Biswas, B. N. Joshi, K. Mahata, A. Shrivastava, R. P. Vind, S. Pal, B. R. Behera, and V. Singh, Phys. Rev. C **92**, 041601(R) (2015).

[28] C. Sahm, H. Clerc, K.-H. Schmidt, W. Reisdorf, P. Armbruster, F. Hessberger, J. Keller, G. Münzenberg, and D. Vermeulen, Nucl. Phys. A **441**, 316 (1985).

[29] V. Singh, B. R. Behera, M. Kaur, A. Kumar, K. P. Singh, N. Madhavan, S. Nath, J. Gehlot, G. Mohanto, A. Jhingan, I. Mukul, T. Varughese, J. Sadhukhan, S. Pal, S. Goyal, A. Saxena, S. Santra, and S. Kailas, Phys. Rev. C **89**, 024609 (2014).

[30] A. Junghans, M. de Jong, H.-G. Clerc, A. Ignatyuk, G. Kudyaev, and K.-H. Schmidt, Nucl. Phys. A **629**, 635 (1998).

[31] G. Fazio, G. Giardina, G. Mandaglio, R. Ruggeri, A. I. Muminov, A. K. Nasirov, Y. T. Oganessian, A. G. Popeko, R. N. Sagaidak, A. V. Yeremin, S. Hofmann, F. Hanappe, and C. Stodel, Phys. Rev. C **72**, 064614 (2005).

[32] K. Kim, Y. Kim, A. K. Nasirov, G. Mandaglio, and G. Giardina, Phys. Rev. C **91**, 064608 (2015).

[33] H.-G. Clerc, J. Keller, C.-C. Sahm, K.-H. Schmidt, H. Schulte, and D. Vermeulen, Nucl. Phys. A **419**, 571 (1984).

[34] N. Madhavan, S. Nath, T. Varughese, J. Gehlot, A. Jhingan, P. Sugathan, A. K. Sinha, R. Singh, K. M. Varier, M. C. Radhakrishna, E. Prasad, S. Kalkal, G. Mohanto, J. J. Das, R. Kumar, R. P. Singh, S. Muralithar, R. K. Bhowmik, A. Roy, S. K. Suman, A. Mandal, T. S. Datta, J. Chacko, A. Choudhury, U. G. Naik, M. Malyadri, A. J.and Archunan, J. Zacharias, S. Rao, P. Mukesh Kumar, Barua, E. T. Subramanian, K. Rani, B. P. Ajith Kumar, and K. S. Golda, Pramana **75**, 317 (2010).

[35] T. Banerjee, S. Abhilash, D. Kabiraj, S. Ojha, G. Umapathy, M. Shareef, P. Laveen, H. Duggal, R. Amarnadh, J. Gehlot, S. Nath, and D. Mehta, Vacuum **144**, 190 (2017).

[36] S. Nath, A Monte Carlo code to model ion transport in dilute gas medium (unpublished).

[37] E. Prasad, K. M. Varier, N. Madhavan, S. Nath, J. Gehlot, S. Kalkal, J. Sadhukhan, G. Mohanto, P. Sugathan, A. Jhingan, B. R. S. Babu, T. Varughese, K. S. Golda, B. P. Ajith Kumar, B. Satheesh, S. Pal, R. Singh, A. K. Sinha, and S. Kailas, Phys. Rev. C **84**, 064606 (2011).

[38] P. V. Laveen, E. Prasad, N. Madhavan, S. Pal, J. Sadhukhan, S. Nath, J. Gehlot, A. Jhingan, K. M. Varier, R. G. Thomas, A. M. Vinodkumar, A. Shamlath, T. Varughese, P. Sugathan, B. R. S. Babu, S. Appannababu, K. S. Golda, B. R. Behera, V. Singh, R. Sandal, A. Saxena, B. V. John, and S. Kailas, J. Phys. G: Nucl. Part. Phys. **42**, 095105 (2015).

[39] http://www.iuac.res.in/NIAS/.

[40] S. Nath, P. V. M. Rao, S. Pal, J. Gehlot, E. Prasad, G. Mohanto, S. Kalkal, J. Sadhukhan, P. D. Shidling, K. S. Golda, A. Jhingan, N. Madhavan, S. Muralithar, and A. K. Sinha, Phys. Rev. C **81**, 064601 (2010).

[41] G. Mohanto, N. Madhavan, S. Nath, J. Gehlot, I. Mukul, A. Jhingan, T. Varughese, A. Roy, R. K. Bhowmik, I. Mazumdar, D. A. Gothe, P. B. Chavan, J. Sadhukhan, S. Pal, M. Kaur, V. Singh, A. K. Sinha, and V. S. Ramamurthy, Phys. Rev. C **88**, 034606 (2013).

[42] J. Gehlot, A. M. Vinodkumar, N. Madhavan, S. Nath, A. Jhingan, T. Varughese, T. Banerjee, A. Shamlath, P. V. Laveen, M. Shareef, P. Jisha, P. S. Devi, G. N. Jyothi, M. M. Hosamani, I. Mazumdar, V. I. Chepigin, M. L. Chelnokov, A. V. Yeremin, A. K. Sinha, and B. R. S. Babu, Phys. Rev. C **99**, 034615 (2019).

[43] A. Nasirov, A. Fukushima, Y. Toyoshima, Y. Aritomo, A. Muminov, S. Kalandarov, and R. Utamuratov, Nucl. Phys. A **759**, 342 (2005).

[44] A. K. Nasirov, G. Giardina, G. Mandaglio, M. Manganaro, F. Hanappe, S. Heinz, S. Hofmann, A. I. Muminov, and W. Scheid, Phys. Rev. C **79**, 024606 (2009).

[45] G. Giardina, S. Hofmann, A. I. Muminov, and A. K. Nasirov, Eur. Phys. J. A **8**, 205 (2000).

[46] G. Fazio, G. Giardina, F. Hanappe, G. Mandaglio, M. Manganaro, I. A. Muminov, A. K. Nasirov, and C. Saccá, J. Phys. Soc. Jpn. **77**, 124201 (2008).

[47] G. Fazio, G. Giardina, A. Lamberto, R. Ruggeri, C. Saccà, R. Palamara, A. I. Muminov, A. K. Nasirov, U. T. Yakhshiev, F. Hanappe, T. Materna, and L. Stuttgé, J. Phys. Soc. Jpn. **72**, 2509 (2003).

[48] B. Borderie, M. Berlanger, D. Gardès, F. Hanappe, L. Nowicki, J. Peter, and B. Tamain, Z. Phys. A **299**, 263 (1981).

[49] G. Mandaglio, G. Fazio, G. Giardina, F. Hanappe, M. Manganaro, A. K. Nasirov, and C. Sacca, Phys. At. Nucl. **72**, 1639 (2009).

[50] A. K. Nasirov, G. Mandaglio, G. Giardina, A. Sobiczewski, and A. I. Muminov, Phys. Rev. C **84**, 044612 (2011).

[51] A. K. Nasirov, A. I. Muminov, R. K. Utamuratov, G. Fazio, G. Giardina, F. Hanappe, G. Mandaglio, M. Manganaro, and W. Scheid, Eur. Phys. J. A **34**, 325 (2007).

[52] G. Audi and A. Wapstra, Nucl. Phys. A **595**, 409 (1995).

[53] P. Moller, J. Nix, W. Myers, and W. Swiatecki, At. Data Nucl. Data Tables **59**, 185 (1995).

[54] G. Mandaglio, G. Giardina, A. K. Nasirov, and A. Sobiczewski, Phys. Rev. C **86**, 064607 (2012).

[55] A. J. Sierk, Phys. Rev. C **33**, 2039 (1986).

[56] P. Vergani, E. Gadioli, E. Vaciago, E. Fabrici, E. Gadioli Erba, M. Galmarini, G. Ciavola, and C. Marchetta, Phys. Rev. C **48**, 1815 (1993).

[57] S. Chakrabarty, B. Tomar, A. Goswami, G. Gubbi, S. Manohar, A. Sharma, B. Bindukumar, and S. Mukherjee, Nucl. Phys. A **678**, 355 (2000).

[58] F. Hessberger, V. Ninov, D. Ackermann, and A. Lüttgen, Nucl. Phys. A **568**, 121 (1994).

[59] https://www.gsi.de/work/forschung/nustarenna/nustarenna_divisions/she_physik/experimental_setup/ship.htm.

[60] M. Trotta, A. Stefanini, S. Beghini *et al.*, Eur. Phys. J. A **25**, 615 (2005).

[61] P. Shidling, N. Madhavan, V. Ramamurthy, S. Nath, N. Badiger, S. Pal, A. Sinha, A. Jhingan, S. Muralithar, P. Sugathan, S. Kailas, B. Behera, R. Singh, K. Varier, and M. Radhakrishna, Phys. Lett. B **670**, 99 (2008).

[62] D. J. Hinde, R. du Rietz, M. Dasgupta, R. G. Thomas, and L. R. Gasques, Phys. Rev. Lett. **101**, 092701 (2008).

[63] R. Rafiei, R. G. Thomas, D. J. Hinde, M. Dasgupta, C. R. Morton, L. R. Gasques, M. L. Brown, and M. D. Rodriguez, Phys. Rev. C **77**, 024606 (2008).

[64] E. Prasad, K. M. Varier, R. G. Thomas, P. Sugathan, A. Jhingan, N. Madhavan, B. R. S. Babu, R. Sandal, S. Kalkal, S. Appannababu, J. Gehlot, K. S. Golda, S. Nath, A. M. Vinodkumar, B. P. Ajith Kumar, B. V. John, G. Mohanto, M. M. Musthafa, R. Singh, A. K. Sinha, and S. Kailas, Phys. Rev. C **81**, 054608 (2010).

[65] R. G. Thomas, D. J. Hinde, D. Duniec, F. Zenke, M. Dasgupta, M. L. Brown, M. Evers, L. R. Gasques, M. D. Rodriguez, and A. Diaz-Torres, Phys. Rev. C **77**, 034610 (2008).

[66] N. V. Antonenko, E. A. Cherepanov, A. K. Nasirov, V. P. Permjakov, and V. V. Volkov, Phys. Rev. C **51**, 2635 (1995).